39th IAHR WORLD CONGRESS GRANADA, SPAIN 2022 From Snow to Sea 19-24 June 2022

Proceedings of the 39th IAHR World Congress
19–24 June 2022, Granada, Spain
doi://10.3850/IAHR-39WC2521716X2022444

Flow development in rough-bed open channels

Andrea Zampiron[(1)], Stuart Cameron[(1)], Mark Stewart[(1)] and Vladimir Nikora[(1)]

[(1)] University of Aberdeen, Aberdeen, United Kingdom
andrea.zampiron@abdn.ac.uk

Abstract

In open-channel flows, one of the main assumptions is of fully developed flow, which means that flow parameters do not change in the streamwise direction. The question then is: what distance from the flume entrance is required to achieve fully developed flow conditions? The available data are not sufficient to answer this question properly, and researchers often employ some rather intuitive approximations instead of tailored preliminary measurements. This paper assesses the development of the flow in two different facilities using a combination of stereoscopic particle-image velocimetry and acoustic Doppler velocimetry data sets covering a range of flow conditions and bed roughness. It is found that while some turbulence features are essentially fully developed within 100 flow depths (H) from the channel entrance (i.e., mean velocity, Reynolds stresses, and large-scale motions), others require distances up to 150H (i.e., streamwise turbulent variance and very large-scale motions).

Keywords: Hydraulic experiments; Open-channel flow; Turbulence; Flow development; Very-large-scale motions

1. INTRODUCTION

A uniform open channel flow (OCF) is fully developed if flow quantities do not change in the streamwise direction. The streamwise development of the flow in open channels to the point where it is fully developed is an important aspect of the experimental design that is often underestimated, or even overlooked. To ensure comparability across studies, experiments should be conducted in the fully developed flow region.

The distance from the channel entrance to the point where the flow is fully developed is denoted as flow development length (L_D). Previous works (e.g., Yalin, 1977; Kirkgöz and Ardiçlioğlu, 1997; Nikora et al., 1998; Ranga Raju et al., 2000; Wilkerson et al., 2019) suggest L_D in the range 40-100H depending on the flow conditions. These works studied the development of a narrow range of flow quantities, mostly velocity mean values and standard deviation only. However, the analysis of a wider range of flow quantities can provide a more conscious assessment of L_D. In some situations, we may choose to rely on a subset of parameters (e.g., mean velocity) depending on the problem at hand.

The goal of this paper is to study the development of open-channel flows (OCFs) for the case of uniform flow in wide channels. Stereoscopic particle image velocimetry (PIV) and acoustic Doppler velocimetry (ADV) measurements were carried out for a range of bed roughness and flow conditions. We explore the streamwise evolution of mean velocity, streamwise variance, Reynolds stresses, and large- and very large-scale motions (LSMs and VLSMs, respectively, e.g., Cameron et al., 2017). In the next section, open-channel facilities, bed roughness and the experimental setups are described. The main results are reported in section 3, whereas the key findings of this work are briefly summarised in section 4.

2. EXPERIMENTAL DATASETS

The data presented in this paper were collected in the Fluid Mechanics Laboratory of the University of Aberdeen using two facilities: the Aberdeen Open-Channel Facility (AOCF, e.g., Cameron et al., 2017); and the 'RS' open-channel flume (e.g., Zampiron et al., 2020). Both channels featured a rectangular cross section with glass sidewalls, adjustable slope, and vertical slat weirs at the exit section to regulate the backwater curve. The AOCF flume is 1.18 m wide and 18 m long, whereas the RS flume is a smaller facility with a width (B) of 0.4 m and a working length of 10.75 m. Water was circulated by centrifugal pumps, while a series of honeycomb panels and vertical guide vanes at the entrance of the flumes removed large-scale turbulence, ensuring uniformly distributed flow as it entered the channel.

Different types of bed roughness were explored: three types of self-affine (SA) fractal surfaces (Nikora et al., 2019; Stewart et al., 2019), glass spheres (GSs, Cameron et al., 2017) and micro hooks (MHs, Zampiron et al., 2020). The three SA roughness patterns feature different scaling exponents $-\beta$ of the surface elevation spectra, with $-\beta = 1$ (SA1), $-\beta = 5/3$ (SA2) and $-\beta = 3$ (SA3), having the same roughness height $\Delta = 6$ mm, where Δ is equal to four standard deviations of the bed roughness elevations. The glass spheres had a diameter of Δ = 16 mm, whereas the micro hooks had a height of Δ = 1.1 mm.

The data were collected using PIV and ADV at different locations along the two flumes. The SA (PIV and ADV) and the GS (PIV only) roughness types were studied in the AOCF flume, while the MH roughness case was tested in the RS flume (ADV only). In the ADV runs, velocity was measured at z/H = 0.3 at different positions along the channels (z is elevation from the mean bed and H is mean flow depth), with a sampling frequency of 100 Hz and a duration of 8 hours. For details on the PIV measurements for the GS and SA roughness see Stewart (2014) and Nikora et al. (2019), respectively.

All flows were uniform (within the fully developed sections of the facilities), turbulent (Reynolds number $Re = UH/\nu \gg 1$, U is flow bulk velocity and ν is kinematic viscosity), subcritical (Froude number $Fr = U/\sqrt{gH} < 1$, g is gravity acceleration) and statistically steady. Hydraulic conditions of the experiments are presented in Tables 1 and 2. Superscript '+' denoted normalisation by the viscous length scale ν/u_*, where $u_* = \sqrt{gHS_b}$ is shear velocity and S_b is bed slope. Same labels are used for runs sharing same nominal flow conditions.

Table 1 Flow conditions for the PIV experiments in AOCF

RUN	H (mm)	S_b (%)	u_* (m s^{-1})	U (m s^{-1})	Re (-)	Fr (-)	B/H (-)	H/Δ (-)	H^+ (-)	Δ^+ (-)
SA1_H080	80.1	0.076	0.024	0.267	21400	0.30	14.7	13.3	1960	147
SA1_H120	120.3	0.050	0.024	0.291	35000	0.27	9.8	20.1	2930	146
SA2_H080	79.8	0.076	0.024	0.266	21200	0.30	14.8	13.3	1950	147
SA2_H120	119.9	0.050	0.024	0.293	35100	0.27	9.8	20.0	2910	146
SA3_H080	79.9	0.076	0.024	0.305	24400	0.34	14.8	13.3	1950	147
SA3_H120	120.4	0.050	0.024	0.323	38900	0.30	9.8	20.1	2930	146
GS_H128	127.3	0.150	0.043	0.494	62800	0.44	9.3	8.0	5510	692

Table 2 Flow conditions for the ADV experiments in AOCF and RS flumes

RUN	H (mm)	S_b (%)	u_* (m s^{-1})	U (m s^{-1})	Re (-)	Fr (-)	B/H (-)	H/Δ (-)	H^+ (-)	Δ^+ (-)
SA1_H080	80.1	0.076	0.024	0.264	21100	0.30	14.7	13.3	1960	147
SA1_H120	120.0	0.050	0.024	0.290	34900	0.27	9.8	20.0	2920	146
SA2_H080	80.3	0.076	0.024	0.267	21500	0.30	14.7	13.4	1970	147
SA2_H120	120.6	0.050	0.024	0.291	35000	0.27	9.8	20.1	2940	146
SA3_H080	80.5	0.076	0.024	0.304	24500	0.34	14.7	13.4	1980	147
SA3_H120	120.3	0.050	0.024	0.321	38600	0.30	9.8	20.1	2930	146
MH_H080	80.2	0.106	0.029	0.378	30300	0.43	5.0	72.9	2320	32

3. RESULTS

Figure 1a-c shows vertical distributions of double-averaged (time- and space-averaged, denoted by overbar and angle brackets, respectively, e.g., Nikora et al., 2007) velocity statistics, normalised with the shear velocity, at selected locations in the streamwise direction (x). The spatial averaging domains are thin slabs parallel to the mean bed with spatial extent well exceeding the scale of bed roughness but being small compared to the scale of the streamwise flow development. The flow entering the channel features low turbulence levels, thus, the spatially averaged Reynolds stress distribution $-\langle\overline{u'w'}\rangle(z)$ (Figure 1c, i.e., prime denotes time fluctuations, and u and w are streamwise and vertical velocity components) can be used to detect the upper edge of the internal boundary layer originated at the entrance as the border between near-zero stress and turbulent flow regions. In our study, a threshold value $-\langle\overline{u'w'}\rangle/u_*^2$ = 0.05 is adopted. The flow region above the boundary layer is shaded grey in Figure 1a-c. The boundary layer grows in thickness with x/H and covers the entire flow depth by x/H = 40. Velocity statistics continue to evolve and approach their fully developed values over larger distances.

The change of the normalised water surface velocity $\langle\bar{u}\rangle^*(z_{ws})$ (z_{ws} is water surface elevation) with x/H is illustrated in Figure 1d, where superscript * denotes normalisation with a corresponding value within the fully developed part of the flow. The velocity data collapse reasonably well for all cases, indicating negligible effects of bed roughness type and relative submergence. Streamwise distributions of $\langle\bar{u}\rangle^*(z_{ws})$ exhibit a maximum at $x/H \approx$ 40, close to the location where the internal boundary layer reaches the water surface. Then $\langle\bar{u}\rangle^*(z_{ws})$ gradually decreases and becomes practically constant at $x/H \gtrapprox$ 100. A similar 'velocity overshoot' has been previously observed in pipes (e.g., Bradshaw, 1971), and can be explained by mass conservation. The reduction of the free-surface velocity downstream reflects the evolution of the turbulence structure towards equilibrium.

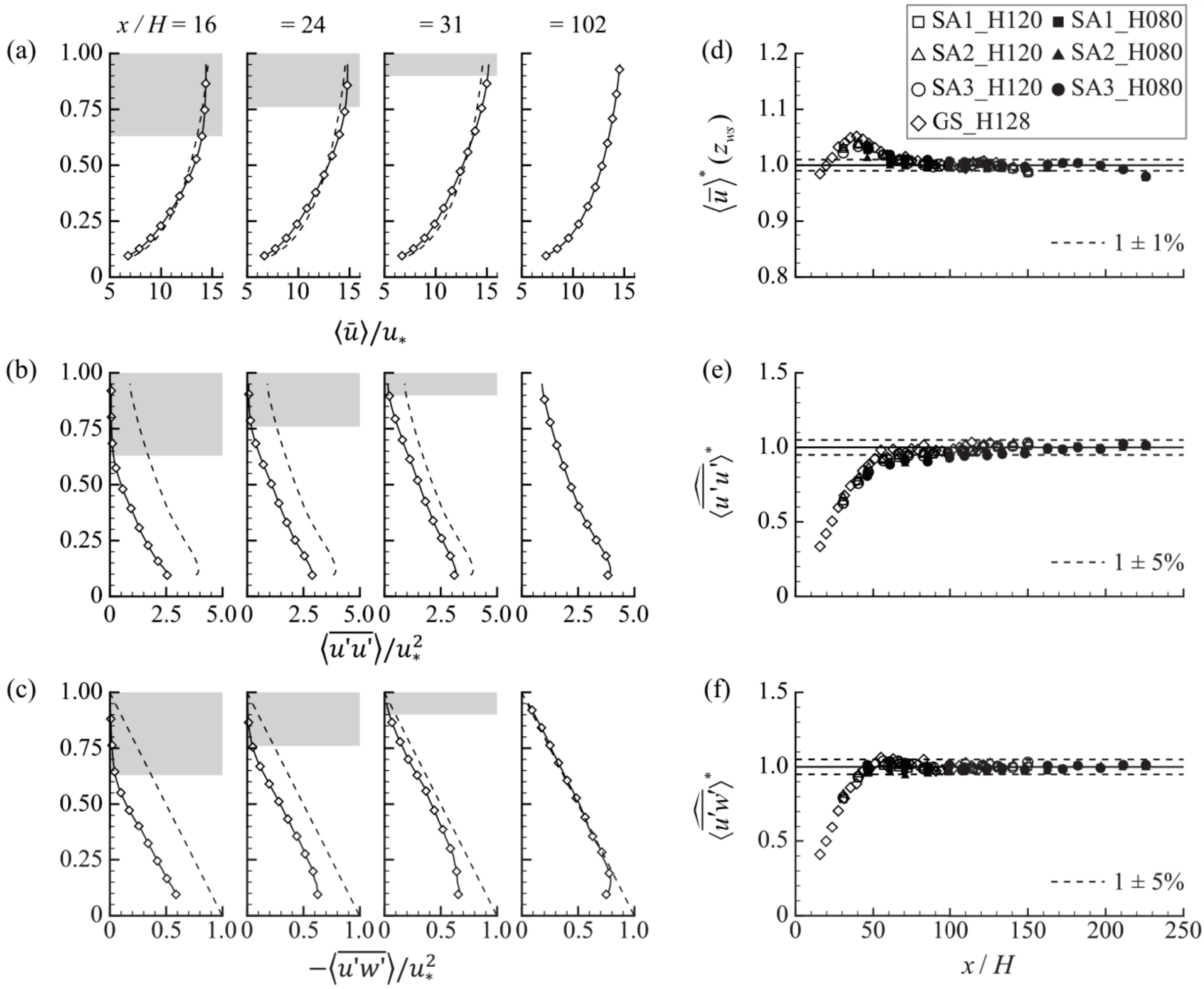

Figure 1. Vertical distributions of spatially averaged: (a) time-averaged streamwise velocity, (c) streamwise turbulent variance and (c) Reynolds stresses for run GS_H128 at different streamwise locations; streamwise distributions of: (d) double-averaged water surface streamwise velocity, (e) depth-averaged turbulent variance and (f) depth-averaged Reynolds stresses. Dashed lines in (a) represent $gS_b(z_{ws} - z)/u_*^2$, whereas in (b-c) they show vertical profile of each statistic at $x/H = 102$ for comparison. Grey areas in (a-c) show flow regions above the developing internal boundary layer. Superscript * in (d-f) denotes normalisation on established values.

Depth-averaged (denoted by hat) streamwise variance $\widehat{\langle \overline{u'u'} \rangle}^*$ (Figure 1e) continues to increase monotonically up to $x/H \approx 150$, whereas depth-averaged Reynolds stresses (Figure 1f) appear to establish at $x/H \approx 100$, after reaching a peak value at $x/H \approx 60$. Development of the streamwise velocity variance is further analysed using pre-multiplied spectra $k_x S_{uu}(k_x)$ in Figure 2a for the case MH_H080 (Table 2). The spectra were computed in the frequency domain and transformed to the wavelength domain using Taylor's frozen turbulence hypothesis $\lambda_x = 2\pi/k_x = \bar{u}/f$, where k_x is streamwise wavenumber, λ_x is streamwise wavelength and f is frequency. Larger wavelengths associated with VLSMs develop at a slower rate compared to smaller wavelength structures (LSMs). Indeed, while the streamwise variance associated with LSMs ($\lambda_x < 10H$, not shown) is well established by $x/H \approx 100$, VLSMs' energy ($\lambda_x > 10H$, Figure 2b) continues to increase up to $x/H \approx 150$, supporting the trend of the total streamwise variance observed in Figure 1e.

4. CONCLUSIONS

In this work, we studied the development of OCFs for a range of bed roughness and hydraulic conditions. The change in mean flow and turbulence statistics along the streamwise coordinate was explored using PIV and ADV measurements. The data suggest that the internal boundary layer generated at the channel entrance covers the entire flow depth by $x \approx 40H$, where time-averaged streamwise velocity at the

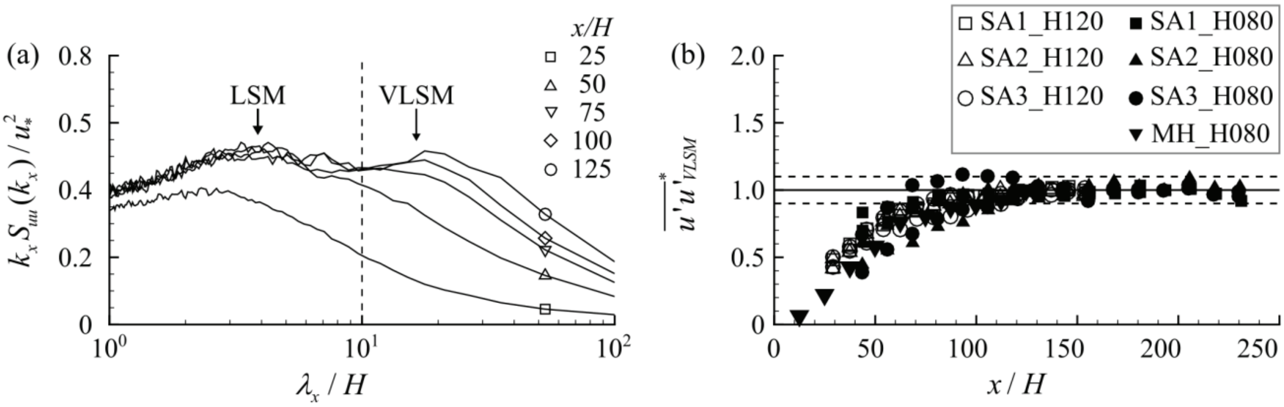

Figure 2. (a) pre-multiplied spectra for run MH_H080 at selected streamwise locations and (b) streamwise distributions of streamwise velocity variance associated with VLSMs ($\lambda_x > 10H$). Superscript * denotes normalisation on established values. Dashed line at $\lambda_x/H = 10$ separates the energy associated with LSMs and VLSMs.

water surface is maximum. Mean flow, Reynolds stresses and LSMs continue to develop downstream, reaching fully developed conditions by around $x \approx 100H$. However, streamwise velocity variance, and VLSMs may require even longer development lengths of $150H$. No measurable effect of relative submergence or roughness type was observed.

Our results suggest that caution should be applied in interpreting distributions of mean velocities and turbulence parameters reported in the literature, as many studies do not provide sufficient details on the measurement location, or they present data measured at streamwise distances from the flume entrance substantially smaller than $100H$. As a rule of thumb, we propose that for uniform OCFs the experimental design should involve turbulence measurements at distances from the channel entrance of around $100H$ or larger. This value significantly exceeds the 40-50H typically assumed. Note that even longer distances may be required in the case undesired patterns are introduced in the incoming flow by unfavourable entrance conditions.

In the near future, we aim to expand this study to an even wider range of flow quantities, including statistics for all three velocity components, higher order statistical moments and secondary currents.

5. ACKNOWLEDGEMENTS

The authors wish to express their gratitude to Roy Gillanders for the help provided. Financial support was provided by three EPSRC/UK grants: ‘High-resolution numerical and experimental studies of turbulence-induced sediment erosion and near-bed transport’ (EP/G056404/1), ‘Bed friction in rough-bed free-surface flows: a theoretical framework, roughness regimes, and quantification’ (EP/K041088/1) and ‘Secondary currents in turbulent flows over rough walls’ (EP/V002414/1).

6. REFERENCES

Bradshaw, P. (1971). An introduction to turbulence and its measurement. Oxford, UK: Pergamon Press.

Cameron, S. M., Nikora, V. I., and Stewart, M. T. (2017). Very-large-scale motions in rough-bed open-channel flow. *Journal of Fluid Mechanics*, 814, 416-429. doi:10.1017/jfm.2017.24

Kirkgöz, M. S., and Ardiçlioğlu, M. (1997). Velocity profiles of developing and developed open channel flow. *Journal of Hydraulic Engineering,* 123(12), 1099-1105. doi:10.1061/(ASCE)0733-9429(1997)123:12(1099)

Nikora, V. I., Goring, D. G., and Biggs, B. J. F. (1998). Silverstream eco-hydraulics flume: Hydraulic design and tests. *New Zealand Journal of Marine and Freshwater Research,* 32(4), 607-620. doi:10.1080/00288330.1998.9516848

Nikora, V., McEwan, I., McLean, S., Coleman, S., Pokrajac, D., and Walters, R. (2007). Double-averaging concept for rough-bed open-channel and overland flows: Theoretical background. *Journal of Hydraulic Engineering,* 133(8), 873-883. doi:10.1061/(ASCE)0733-9429(2007)133:8(873)

Nikora, V. I., Stoesser, T., Cameron, S. M., Stewart, M., Papadopoulos, K., Ouro, P., and Falconer, R. A. (2019). Friction factor decomposition for rough-wall flows: Theoretical background and application to open-channel flows. *Journal of Fluid Mechanics,* 872, 626-664. doi:10.1017/jfm.2019.344

Ranga Raju, K. G., Asawa, G. L., and Mishra, H. K. (2000). Flow-establishment length in rectangular channels and ducts. *Journal of Hydraulic Engineering,* 126(7), 533-539. doi:10.1061/(ASCE)0733-9429(2000)126:7(533)

Stewart, M. T. (2014). Turbulence structure in rough-bed open-channel flow. PhD thesis, University of Aberdeen, UK.

Stewart, M. T., Cameron, S. M., Nikora, V. I., Zampiron, A., and Marusic, I. (2019). Hydraulic resistance in open-channel flows over self-affine rough beds. *Journal of Hydraulic Research,* 57(2), 183-196. doi:10.1080/00221686.2018.1473296

Wilkerson, G., Sharma, S., and Sapkota, D. (2019). Length for uniform flow development in a rough laboratory flume. *Journal of Hydraulic Engineering,* 145(1), 06018018. doi:10.1061/(ASCE)HY.1943-7900.0001554

Yalin, M.S. (1977). Mechanics of sediment transport. 2nd Edition. Oxford, UK: Pergamon Press

Zampiron, A., Cameron, S., and Nikora, V. (2020). Secondary currents and very-large-scale motions in open-channel flows over streamwise ridges. *Journal of Fluid Mechanics,* 887, A17. doi:10.1017/jfm.2020.8

